THE ASTRONOMICAL JOURNAL, 116:429–439, 1998 July
© 1998. The American Astronomical Society. All rights reserved. Printed in U.S.A.

PHOTOMETRY OF PROXIMA CENTAURI AND BARNARD'S STAR USING *HUBBLE SPACE TELESCOPE* FINE GUIDANCE SENSOR 3: A SEARCH FOR PERIODIC VARIATIONS[1]

G. FRITZ BENEDICT,[2] BARBARA MCARTHUR,[2] E. NELAN,[3] D. STORY,[2,4] A. L. WHIPPLE,[2,5] P. J. SHELUS,[2]
W. H. JEFFERYS,[6] P. D. HEMENWAY,[7] OTTO G. FRANZ,[8] L. H. WASSERMAN,[8]
R. L. DUNCOMBE,[9] W. VAN ALTENA,[10] AND L. W. FREDRICK[11]
Received 1998 January 26; revised 1998 March 16

ABSTRACT

We have observed Proxima Centauri and Barnard's star with the *Hubble Space Telescope* Fine Guidance Sensor 3. Proxima Cen exhibits small-amplitude, periodic photometric variations. Once several sources of systematic photometric error are corrected, we obtain 2 mmag internal photometric precision. We identify two distinct behavior modes over the past 4 years: higher amplitude, longer period and smaller amplitude, shorter period. Within the errors, one period ($P \sim 83$ days) is twice the other. Barnard's star shows very weak evidence for periodicity on a timescale of approximately 130 days. If we interpret these periodic phenomena as rotational modulation of starspots, we identify three discrete spots on Proxima Cen and possibly one spot on Barnard's star. We find that the disturbances change significantly on timescales as short as one rotation period.

Key words: stars: flare — stars: individual (Proxima Centauri, Barnard's star) — stars: late-type — stars: rotation — stars: spots

1. INTRODUCTION

We present photometry of Proxima Centauri and Barnard's star, results ancillary to our astrometric searches for planetary-mass companions (Benedict et al. 1997). Our observations were obtained with Fine Guidance Sensor 3 (FGS 3), a two-axis, white-light interferometer aboard the *Hubble Space Telescope* (*HST*). Bradley et al. (1991) provide an overview of the FGS 3 instrument, and Benedict et al. (1994a) describe the astrometric capabilities of FGS 3 and typical data acquisition strategies. Benedict et al. (1993) assessed FGS 3's photometric qualities and presented the first evidence for periodic variability of Proxima Cen. This latter result was based on 212 days of monitoring. Subsequent data exhibited a period of variation very nearly twice the original (Benedict et al. 1994b). Since that report, we have obtained 14 additional data sets for Proxima Cen and 12 new sets for Barnard's star. The primary value of these observations lies in their precision, not in their temporal span or aggregate numbers. We have previously determined that a 90 s observation obtained with FGS 3 has a 1 σ precision of 0.001 mag at $V = 11$ (Benedict et al. 1993), in the absence of systematic errors.

In this paper we discuss the data sets and assess systematic errors, including background contamination and FGS position-dependent photometric response. We also present a revised photometric flat field. We then exhibit and analyze light curves for Proxima Cen and Barnard's star. We find weak evidence for periodic variations in the brightness of Barnard's star. However, Proxima Cen exhibits significant periodic photometric variations, with changes in amplitude and/or period. We next interpret these variations as rotational modulation of chromospheric structure (starspots and/or plages) and conclude with a brief comparison with other determinations of the rotation rate of Proxima Cen. Tables 1 and 2 provide aliases and physical parameters for our two science targets.

We use the term "pickle" to describe the total field of view of the FGS. The instantaneous field of view of FGS 3 is a $5'' \times 5''$ square aperture. Figure 1 shows a finding chart for the Barnard's star reference frame in the FGS 3 pickle as observed on 1994 August 6. Benedict et al. (1993) contains a finding chart for the Proxima Cen reference frame.

2. DATA REDUCTION

2.1. *The Data*

All position and brightness measurements from FGS 3 are comprised of series of 0.025 s samples (i.e., 40 Hz data rate), of between 20 and 120 s or $\sim$600 s duration. Each FGS contains four photomultipliers (PMTs), two for each axis. We sum the output of all four to produce our measurement, S, the average count per 0.025 s sample, obtained during the entire exposure. The coverage for both targets suffers from extended gaps, due to *HST* pointing constraints (described by Benedict et al. 1993) and other scheduling difficulties. The filter (F583W) has a bandpass centered on 583 nm, with 234 nm FWHM.

For Proxima Cen, the data now include 152 shorter exposures secured over 4 years (1992 March to 1997 October) and 15 longer exposures (1995 July to 1996 July).

[1] Based on observations with the NASA/ESA *Hubble Space Telescope*, obtained at the Space Telescope Science Institute, which is operated by the Association of Universities for Research in Astronomy, Inc., under NASA contract NAS 5-26555.

[2] McDonald Observatory, University of Texas at Austin, Austin, TX 78712.
[3] Space Telescope Science Institute, 3700 San Martin Drive, Baltimore, MD 21218.
[4] Current address: Jackson and Tull, Inc., Suite 200, 7375 Executive Place, Seabrook, MD 20706.
[5] Current address: AlliedSignal Aerospace, P.O. Box 91, Annapolis Junction, MD 20701.
[6] Department of Astronomy, RLM 15.308, University of Texas at Austin, Austin, TX 78712.
[7] Department of Physics, University of Rhode Island, Kingston, RI 02881.
[8] Lowell Observatory, 1400 West Mars Hill Road, Flagstaff, AZ 86001.
[9] Department of Aerospace Engineering and Engineering Mechanics, University of Texas at Austin, Austin, TX 78712.
[10] Department of Astronomy, Yale University, P.O. Box 208101, New Haven, CT 06520.
[11] Department of Astronomy, University of Virginia, P.O. Box 3818, Charlottesville, VA 22903.

TABLE 1

PROXIMA CENTAURI

Parameter	Value	Reference
Aliases	α Cen C, GJ 551, V645 Cen	
M_V	15.45 ± 0.1	
$B-V$	1.94	
Spectral type	M5 Ve	1
Mass ($M_\odot$)	0.11	2
Luminosity ($L_\odot$)	0.001	3
Radius ($R_\odot$)	0.15	4

REFERENCES.—(1) Gliese & Jahreiss 1991; (2) Kirkpatrick & McCarthy 1994; (3) Liebert & Probst 1987; (4) Panagi & Mathioudakis 1993.

Each orbit contains from two to four exposures. The longest exposure times pertain only to Proxima Cen observations obtained within continuous viewing zone (CVZ) orbits. These specially scheduled orbits permit ~90 minutes on field, during which Proxima Cen is not occulted by Earth. Table A1 in the Appendix gives times of observation, exposure times, and average counts S for all Proxima Cen photometry.

TABLE 2

BARNARD'S STAR

Parameter	Value	Reference
Aliases	GJ 699, G140-24, LHS 57	
M_V	13.2 ± 0.1	1
$B-V$	1.73	
Spectral type	M4 Ve	2
Mass ($M_\odot$)	0.17	3
Luminosity ($L_\odot$)	0.0046	3
Radius ($R_\odot$)	0.17	

REFERENCES.—(1) Gliese & Jahreiss 1991; (2) Kirkpatrick & McCarthy 1994; (3) Henry & McCarthy 1993.

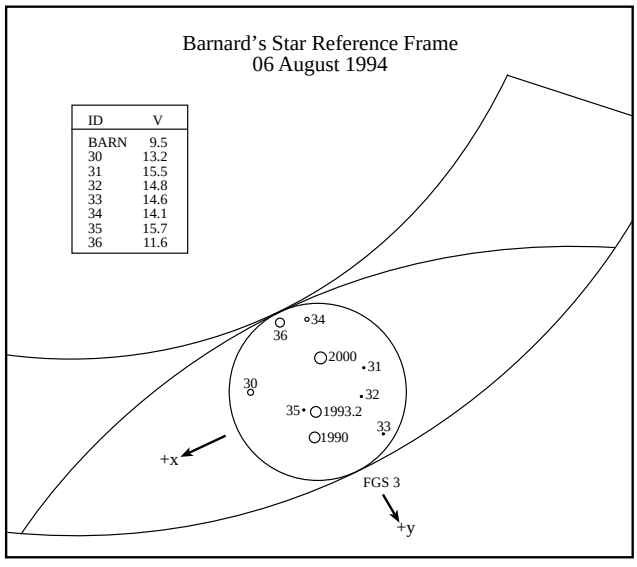

FIG. 1.—The Barnard's star field on 1994 August 4. North is up, east to the left. The pickle coordinate system (X, Y) is indicated. The symbol size is proportional to the relative brightness of each reference star (listed). The central circle (diameter ~3'.8) is accessible by the FGS 3 instantaneous aperture for any *HST* roll. Barnard's star is labeled at three epochs.

Barnard's star was monitored for 3 years (1993 February to 1996 April) and observed three times during each of 35 orbits. Exposures range between 24 and 123 s duration. Table A2 gives times of observation, exposure times, and average counts S for all Barnard's star photometry.

2.2. *Background Light*

We first noted that background contamination might be an issue while assessing the use of astrometric reference stars for photometric flat-fielding. These stars are typically far fainter than the primary science targets. Using them to flat-field the Proxima Cen and Barnard's star photometry introduced a strong 1 yr periodicity (and considerable noise, since they are fainter stars). This problem was not identified in Benedict et al. (1993), since we had access to data spanning less than two-thirds of a year. Figure 2 shows S for two faint reference stars in the Barnard field plotted against angular distance from the Sun. These stars appear brightest when closest to the Sun. Zodiacal light is a source whose brightness depends on the Sun-target separation. The fitting function in Figure 2 is

$$I = A + B \sin(\theta/2), \quad (1)$$

chosen to produce a minimum contribution at $\theta = 180°$. We find $A = 137.1 \pm 0.4$ and $B = -4.1 \pm 0.5$ counts per 25 ms for an average exposure time of 100 s. At a 60° elongation, the contamination amounts to $V = 22.5 \pm 0.3$ mag arcsec^{-2}. The Barnard field is at ecliptic latitude $\beta = +27°$. From a tabulation in Allen (1973), we calculate a signal equivalent to $V = 22.1$ mag arcsec^{-2} for zodiacal light at 60° elongation and ecliptic latitude $\beta = +30°$. The agreement supports our identification of this background source.

We present in Figure 3 an average S for these two Barnard reference stars plotted as a function of time, both uncorrected and corrected for background. These data have been flat-fielded using the time-dependent response function discussed in § 2.3.2 (eq. [2]). Note the reduction in the amplitude of the scatter for the corrected photometry. Presuming zodiacal light as the source, contamination levels are even less for the Proxima Cen observations at ecliptic

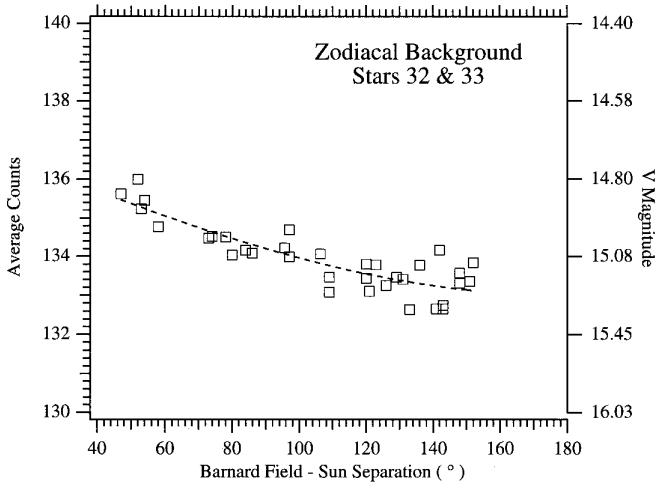

FIG. 2.—S (average counts per 0.025 s) for two faint astrometric reference stars in the Barnard's star field (stars 32 and 33, Fig. 1) vs. target-Sun separation in degrees. The fitting function is eq. (1).

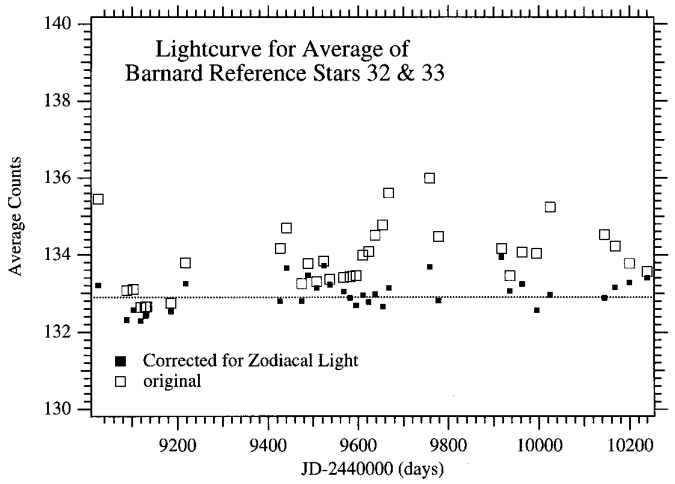

FIG. 3.—Correcting for zodiacal light. Average intensity (S, counts per 0.025 s) vs. MJD for the average of two faint astrometric reference stars in the Barnard's star field (Fig. 2). The horizontal line denotes the mean brightness of the corrected data. Scatter is far less in the corrected data. Uncorrected and corrected values have been flat-fielded with eq. (2).

latitude $\beta = -44°$, introducing a maximum systematic error of 0.0007 mag for a 100 s observation. We conclude that the effects of this component of the background are insignificant for Proxima Cen and Barnard's star photometry.

Should background determination become more important in the future, we note that during an intraorbit observation sequence the PMTs are never turned off. Hence, the *HST* data archive contains PMT measurements taken during slews from one star to the next. The astrometric reduction pipeline at the Space Telescope Science Institute has been modified to provide these background data automatically.

2.3. *Photometric Flat-fielding*

We explore two kinds of flat-fielding: position and time dependent. We first assess whether or not flat-field corrections are necessary and, if so, determine their functional form.

2.3.1. *Position-dependent Photometric Response*

Having discovered that background variations contaminate the photometry of faint astrometric reference stars, we required an alternative source for flat-field data. To maintain the astrometric calibration of FGS 3, a star field in M35 has been measured roughly once per month for the last 4 years. Whipple et al. (1995) describe this continuing astrometric long-term stability (LTSTAB) test. The field, on the ecliptic and, hence, always observed in one of two orientations (fall or spring) flipped by 180°, contains bright stars for which background contamination is negligible. However, an initial application of a time-dependent flat field based on bright M35 stars also introduced a strong 1 yr periodicity.

The positions of the three M35 LTSTAB stars within FGS 3 are shown in Figure 4. The "eye" is bordered by the pickle edge at the two nominal rolls for this field. The central circle (diameter $\sim 3'.8$) is accessible by the FGS 3 instantaneous aperture for any *HST* roll.

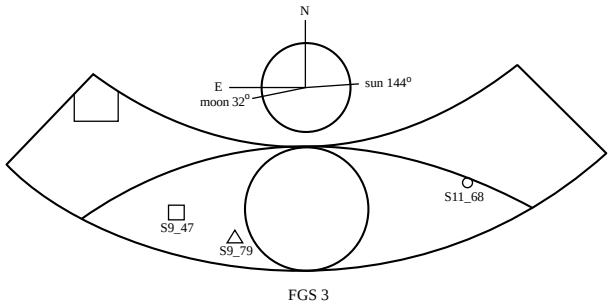

FIG. 4.—Field of view of FGS 3 with the positions of three M35 stars. The V magnitude is given as part of the identification (e.g., S9_47 has $V = 9.47$).

Figure 5 (*bottom*) presents normalized intensities [$I = S(t)/S_{av}$, where S_{av} is determined from the entire run of data] for the three LTSTAB stars as a function of time. The variation of each star has first been modeled as a linear trend. The parameters, intercept (I_0) and slope (I'), are given in Table 3. The resulting residuals (Fig. 5, *top*) have been modeled with a sine wave, constraining $P = 365.25$ days. The residuals have a square-wave periodic structure because, rather than a range of spacecraft rolls, there are only two orientations. The resulting parameters and errors are given in Table 3. In Figure 6, we plot the amplitude of this side-to-side variation against radial distance from the pickle center. For the M35 stars, the farther the star from the pickle center, the larger the roll-induced variation. Figure 6 includes several other 1 yr period amplitudes: a preliminary result for GJ 748 ($V \sim 11.1$, ecliptic latitude $\beta \sim +23°$), always observed in the center of the pickle; the

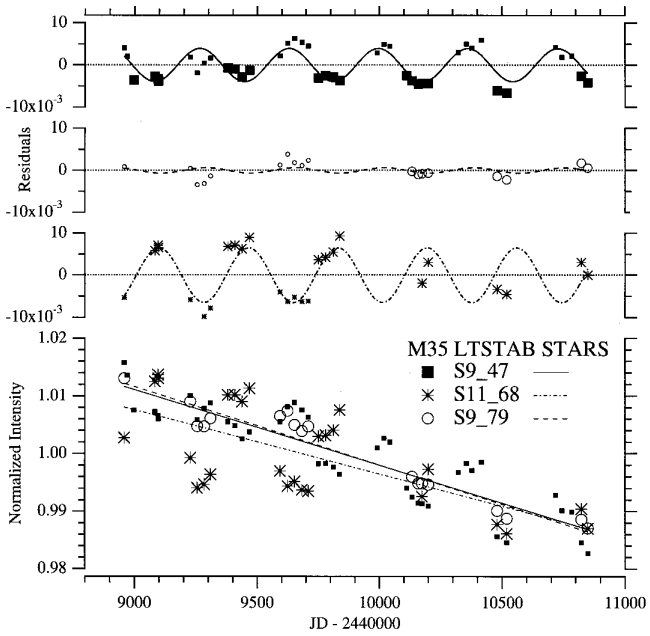

FIG. 5.—Time-dependent photometric variations for three stars in M35, modeled as linear trends whose parameters (I_0 and I') are given in Table 3. The residuals in the top panels are size-coded to show the two LTSTAB orientations (fall = small, spring = large) and fitted with sine functions. Note the differences in the variation amplitude (parameter A in Table 3).

TABLE 3

FLAT-FIELD MODELING: M35 STARS

Parameter	S9_79	S11_68	S9_47
Linear trend:			
I_0 (counts)	1.134 ± 0.008	1.107 ± 0.023	1.129 ± 0.015
I' (10^{-5} counts day^{-1})	-1.36 ± 0.10	-1.11 ± 0.24	-1.31 ± 0.10
Variation from 180° flip:			
A (counts)	0.0006 ± 0.0006	-0.0065 ± 0.0003	0.0039 ± 0.0004
P (days)	365.25 ± 0	365.25 ± 0	365.25 ± 0
ϕ (rad)	281.56 ± 1.03	281.71 ± 0.17	282.00 ± 0.14

Barnard reference star photometry from Figure 3 corrected for background; and photometry of the brightest reference star in the Barnard field (Fig. 1, star 36; $V \sim 11.5$). Figure 6 suggests that within the inscribed circle of Figure 1 ($r < 180''$), position-dependent photometric response variations should be less than 0.002 mag.

We have also identified one high spatial frequency position-dependent flat-field component for FGS 3. Light curves for two of the Barnard reference stars evidenced sudden decreases in brightness with subsequent return to previous levels. The decrease for reference star 34 was 29%; for star 36, 17%. Shown in Figure 7, both decreases occurred in the same location within FGS 3, very near the $-Y$ edge. The pickle coordinates of the center of this area are $(X, Y) = (-25, 627)$. We estimate the size of the low-sensitivity region to be about $10'' \times 10''$. In addition, Proxima Cen reference star observations acquired 1 yr prior to the Barnard reference star observations and within a few arcseconds of this position showed no decrease, providing additional evidence that FGS 3 is not suitable for wide-field, precise photometry of faint stars.

Evidence that the photometric response may vary locally and randomly with time dissuades us from mapping a position-dependent flat field over the entire pickle. However, for bright stars ($V < 11$) observed within $\sim 20''$ of pickle center (Fig. 1), these identified systematics should produce very little effect. *All Proxima Cen and Barnard's star observations were secured within* 15″ *of the pickle center.*

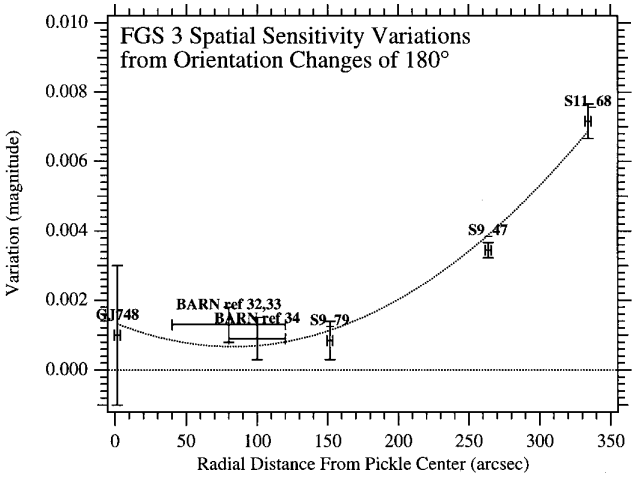

FIG. 6.—Amplitude of side-to-side variation vs. distance from pickle center. Targets are stars from M35 (location from Fig. 4 and amplitude from Fig. 5), stars from the Barnard's star reference frame (Fig. 1), and GJ 748. Error bars along the horizontal axis indicate the radial range within the pickle for all observations of the particular target.

2.3.2. *Time-dependent Photometric Response*

Figure 5 indicates that FGS 3 has become less sensitive with age. For all three LTSTAB stars, the linear trends (I', Table 3) agree within the errors. The apparent 1% drop in sensitivity over 1000 days requires confirmation. Figure 8 presents the time-varying normalized intensity for two other astrometric program stars observed with FGS 3, GJ 623 and GJ 748. Both M dwarfs were observed in pickle center. Comparing the values of I' in Table 3 and Table 4, the rate of decline in brightness for GJ 623 and GJ 748 is identical (within the errors) to that seen in the M35 stars.

A final concern is that the rate of decline of PMT sensitivity might vary with wavelength. The M35 stars (stars 547, 500, and 312 in the catalog of Cudworth 1971) have $0.12 < B-V < 0.49$, while GJ 623 and GJ 748 have $B-V \simeq +1.5$. There appears to be no dependence on color.

The weighted average for five stars from three different fields yields

$$1.131 \pm 0.006 + (1.30 \pm 0.06) \times 10^{-5} \text{ MJD} \qquad (2)$$

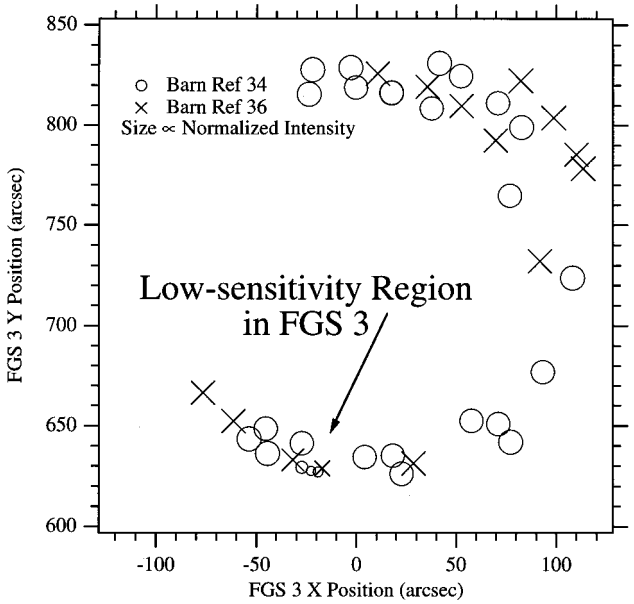

FIG. 7.—Intensities of Barnard field reference stars 34 and 36 plotted against pickle coordinates for all observation dates. The symbol size is proportional to the normalized intensity. The low-sensitivity region is clearly seen in the vicinity of $(X, Y) = (-25, 627)$.

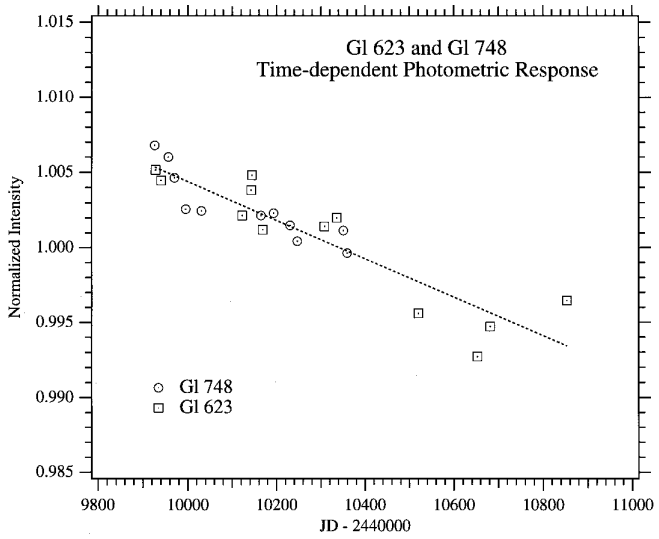

FIG. 8.—Trend of normalized intensity for GJ 623 and GJ 748. The fitted line parameters are given in Table 3.

as the temporal photometric flat field for the pickle center. As an additional test of the reality of this sensitivity decrease, we note that the intensity data for the two astrometric reference stars in the Barnard's star field shown in Figure 3 have been flat-fielded with equation (2). Thus, a total of seven stars from four different fields show similar brightness trends, adequate evidence for a sensitivity loss in FGS 3.

2.4. *Photometric Calibration*

All magnitudes presented in this paper are provisional, since a final calibration from F585W to V is not yet available. If magnitudes are given, they are derived through

$$V = -2.5 \log S + 20.0349 \quad (3)$$

with no color term, where S is the average counts per 0.025 s sample, summed over all four PMTs. No results are based on these provisional calibrated magnitudes. They are provided only as a convenience.

2.5. *Summary: Photometric Error and Photometric Precision*

We have identified sky background (zodiacal light), within-pickle response variations, and time-dependent sensitivity variations as contributing sources of systematic error for our photometry. Since our science targets, Proxima Cen and Barnard's star, are bright, the effect of zodiacal light is at most 0.001 mag. Since we observe these stars only in the pickle center, spatially induced variations are reduced to about 0.001 mag, our claimed per-observation precision at $V \sim 11$. A weighted average of the temporal response of five stars in three fields provides a very precise flat field whose slope error could introduce at most 0.001 mag systematic error over 1000 days. (Since we are doing only differential photometry, we ignore the zero-point error in the flat field.) Combining these sources of error yields a per-observation precision of 0.002 mag.

TABLE 4

FLAT-FIELD MODELING: M DWARF STARS

Parameter	GJ 623 and GJ 748
I_0 (counts).....	1.133 ± 0.0132
I' (10^{-5} counts day^{-1}).....	-1.30 ± 0.13

3. PHOTOMETRIC RESULTS

We apply the flat field (eq. [2]) to the Table A1 and A2 S-values and plot (Proxima Cen, Fig. 9; Barnard's star, Fig. 10) the resulting intensities as a function of MJD (JD $-2{,}440{,}000$). Our coverage in time is not uniform for either target. There are extended gaps in coverage, some due to the *HST* solar constraint (no observations permitted closer than $\pm 50°$ to the Sun). The largest gap, in 1994 for Proxima Cen, was due to an awkward transition from Guaranteed Time Observations to Guest Observer status and a hiatus due to suspected equipment problems.

3.1. *Trends in Brightness*

For Proxima Cen, the solid line in Figure 9 indicates an overall trend of increasing brightness with time. In units of normalized intensity, the rate of change of brightness $[(1.63 \pm 0.37) \times 10^{-5}]$ is similar to that of the adopted flat field (eq. [2]). For Barnard's star (Fig. 10), the slope of the upward trend in units of normalized intensity is $(+0.91 \pm 0.18) \times 10^{-5}$, again suspiciously similar in absolute value to the adopted flat-field relation (eq. [2]). Since seven stars from four different fields exhibit the sensitivity decrease described by the flat field, the Proxima and Barnard upward trends are unlikely to be a flat-field artifact.

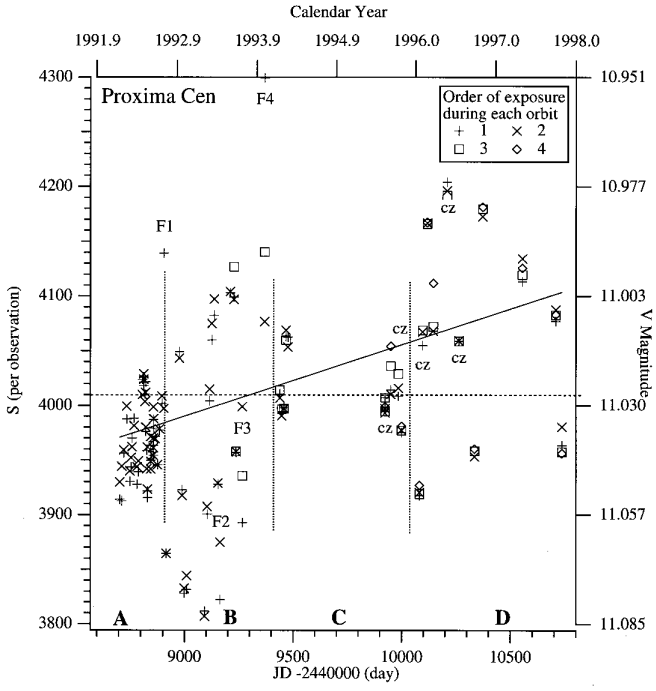

FIG. 9.—Photometry of Proxima Cen. Each orbit contains two, three, or four exposures (Table A1). Exposures perturbed by flares are marked F1–F4. Exposures acquired during CVZ orbits are labeled "cz." Error bars are about the size of the plotted symbols. Four segments and two distinct behavior modes are identified, A–D. The trend line is discussed in the text.

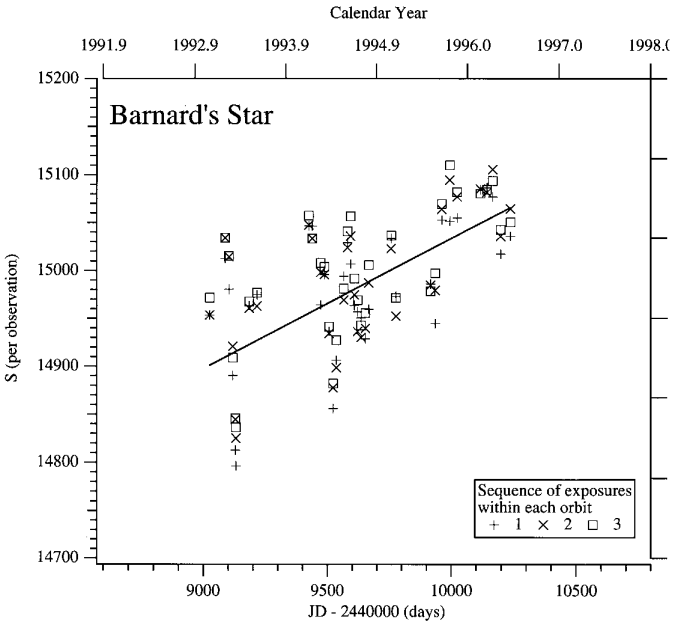

FIG. 10.—Photometry of Barnard's star. Each symbol represents the average of an exposure. Each orbit contains three exposures (Table A2). No flares were detected. Error bars are smaller than the plotted symbols. The timescale is identical to Fig. 9. The trend line is discussed in the text.

A final caveat: Proxima Cen and Barnard's star are somewhat redder (Tables 1 and 2) than GJ 623 and GJ 748. If the sensitivity loss varies with wavelength (e.g., more sensitivity loss for blue than for red wavelengths), it would have to be a very steeply dependent function, showing no effect at $B-V = +1.5$.

3.2. *Proxima Cen*

The flat-fielded photometry for each exposure in each orbit appears in Figure 9. The period and amplitude variations evident in Figure 9 will be discussed in § 4. Our total time on target, obtained by summing the exposure times in Table A1, was 6.6 hr. Proxima Cen is a flare star (V654 Cen), and these data contain exposures "contaminated" by stellar flares (marked F1–F4 in Fig. 9). We identified these events by inspecting the 40 Hz photometric data stream for each observation. An example of flare contamination (including a light curve) can be found in Benedict et al. (1993), which discusses a slow, relatively faint ($\Delta V < -0.10$), and multipeaked flare on MJD 8,906 (F1 in Fig. 9). An explosive flare on MJD 9,266 ($\Delta V \sim 0.6$ mag in 1 s; F3 in Fig. 9) produced astrometric changes in Proxima Cen, analyzed in detail by Benedict et al. (1998). This spectacular event provided the motivation for the subsequent CVZ observations ("cz" in Fig. 9), each permitting 30 minutes of monitoring for flares. The F4 event at MJD 9,368 had a relatively small amplitude ($\Delta V \sim -0.13$) but lasted throughout the entire 130 s exposure, hence its large effect on the exposure. Walker (1981) predicts a flare with intensity similar to F3 once every 31 hr. Thus, while disappointing, it is not surprising that we captured none as bright as the F3 event in our additional 2.5 hr of CVZ on-target monitoring. It may be significant that we saw any flares at all, since even the small-amplitude events have only a 60% chance of occurring during our total monitoring duration. We discuss this further in § 5.1.

Individual observations secured within an orbit and not affected by flaring exhibit an internal consistency at the 0.002 mag level.

3.3. *Barnard's Star*

The flat-fielded photometry for each of the three Barnard's star exposures acquired within each orbit appears in Figure 10. Note that the timescale is exactly that used for Figure 9, to facilitate comparison. Again, note that those observations secured within an orbit exhibit an internal consistency at the 0.002 mag level. We find variations within each orbit, but no obvious flaring activity in the Barnard's star results. Possible period and amplitude variations in the Barnard's star data will be discussed in § 4.2.2.

The scatter within each orbit in Figure 10 is somewhat larger than the previously determined (Benedict et al. 1993) 0.001 mag measurement precision. In particular, we inspected the observations on MJD 9,935 and 9,994 and found only a slight upward slope during the first observation on each date. Since the majority of first observations within each orbit are lower, this intraorbit scatter is most likely an instrumental effect, amounting to about 0.001 mag. The first-observation low bias is sometimes seen in the Proxima Cen data (Fig. 9). Leaving all first observations uncorrected will only slightly enlarge the formal errors for our per-orbit means.

4. ANALYSIS

For subsequent analyses of Proxima Cen, we removed the flare contributions by subjecting the per-orbit average to a pruning process. All exposures obtained during each orbit are presented in Figure 9. If one exposure differs by more than 2.5 σ from the mean for that orbit, it is removed and the mean recalculated. This process results in 71 normal points with associated dispersions (the standard deviations calculated for two, three, or four exposures in each orbit) for Proxima Cen. No exposures were removed from the Barnard's star series, since no intraorbit points (shown in Fig. 10) violated the 2.5 σ criterion. The resulting per-orbit average S-values are presented as direct light curves in Figure 13 (Proxima Cen) and Figure 16 (Barnard's star) below. Forming these normal points provides per-orbit photometric precision better than 0.002 mag for the following analyses.

4.1. *Lomb-Scargle Periodograms*

From Figures 9 and 10, we suspect that there are periodic variations in both the Proxima Cen and Barnard's star photometry. To obtain a preliminary identification of these periodicities, we produce Lomb-Scargle periodograms (Press et al. 1992, § 13.8) from the per-orbit normal points presented in Figure 13 (Proxima Cen) and Figure 16 (Barnard's star).

The most statistically significant period in the Proxima Cen periodogram (Fig. 11) is at $P \sim 83$ days, with a false-positive probability less than 0.1%. The very small peak at $P \sim 42$ days indicates the relative strengths of the period derived from the first 212 days (Benedict et al. 1993) relative to the higher amplitude $P \sim 83$ day period. The false-positive probability for the period derived from only the first 212 days was ~1%. Since the periodogram provides no results for very short periods, we have some concern that we

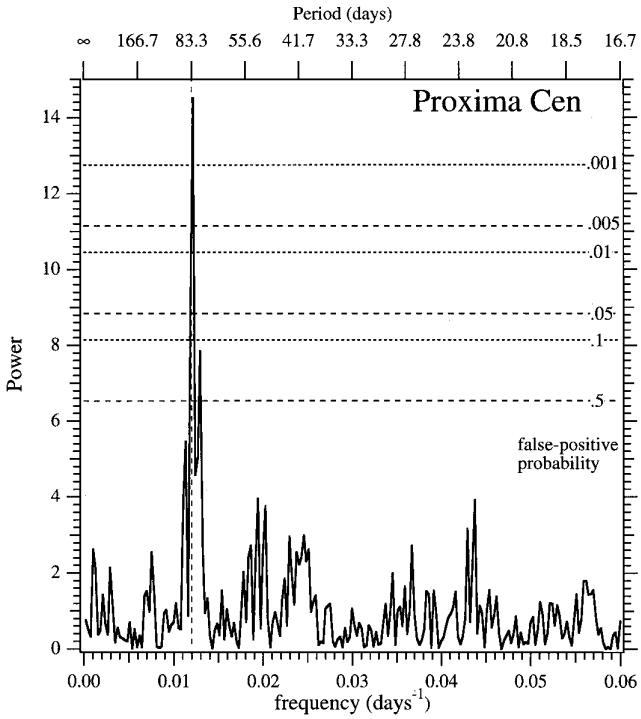

FIG. 11.—Periodogram from 71 normal points (average for each orbit) with flares removed, flat-fielded with eq. (2). The most significant peak is at $P \sim 83$ days, with less than a 0.1% false-positive probability.

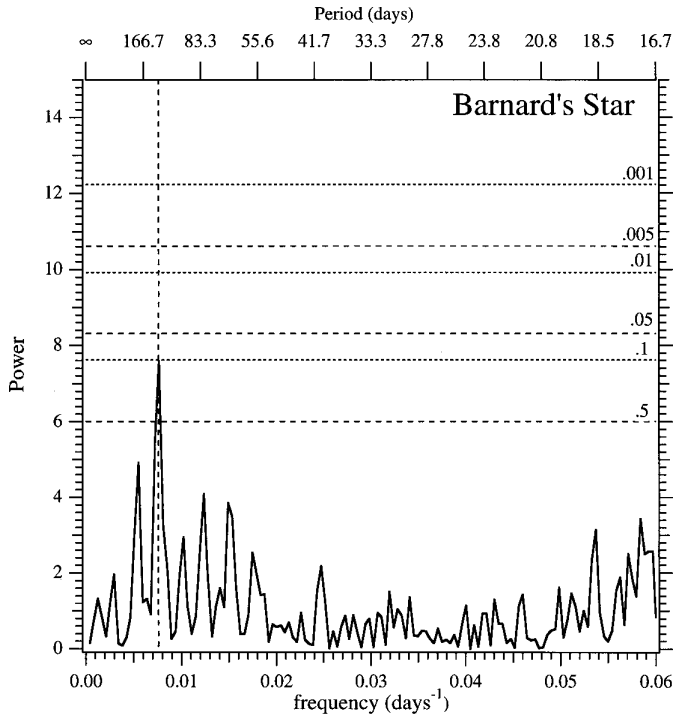

FIG. 12.—Periodogram from 35 normal points (average for each orbit), flat-fielded with eq. (2). The most significant peak is at $P = 130.4$ days, with a 10% false-positive probability.

are undersampling a more rapid variation. We can rule out a range of periods 2 days $< P <$ 20 days from detailed inspection of clusters of data near MJD 8,840 (Fig. 13), where we had a series of observations closely spaced in time (see Table A1).

The periodogram for Barnard's star is shown in Figure 12. The strongest peak (at $P \sim 130$ days) has a 10% false-positive probability. We have much less compelling evidence of variability for Barnard's star than for Proxima Cen.

4.2. *Light Curves*

4.2.1. *Proxima Cen Light Curve*

Given strong support for a periodic variation (periodogram, Fig. 11) and for an overall trend in the brightness (Fig. 9), we model the per-orbit average variations seen in the direct light curve (Fig. 13) with a sine function and trend

$$I = I_0 + I't + A \sin [(2\pi/P)t + \phi] . \quad (4)$$

To reconcile the earlier results (Benedict et al. 1993) with the newer data, we first attempted to model the entire light curve with only two distinct segments, grouping segments B, C, and D together. From the earliest data (segment A) the Proxima Cen photometric variations are characterized by a shorter period and smaller amplitude. Later data are best fitted with a longer period and larger amplitude variation, as evidenced by the periodogram (Fig. 11). Parameters for these fits are listed as A and BCD in Table 5. We find $P_{\rm BCD}/P_A = 1.97 \pm 0.04$.

Noting very large residuals for segment C, we next explored the possibility that Proxima Cen repeats a low-to-high amplitude cycle by fitting the four segments (A–D, Fig. 13) with the same model (eq. [4]). The parameters for these fits are presented in Table 5. Within the errors, $P_A = P_C$ and $P_B = P_D$, with $P_D/P_C = 1.99 \pm 0.02$. A reduction in the number of degrees of freedom by 17% (fitting 71 data points with 20 rather than 10 parameters) reduced the residuals by $\sim$30%. This relative improvement is some support for alternating high- and low-amplitude states. It is also evident that segments A and C have very nearly half the period of segments B and D.

Figure 14 contains phased light curves for the four segments labeled in Figure 13. In the top panel, we show that

TABLE 5

PROXIMA CENTAURI LIGHT-CURVE PARAMETERS

Segment	N	I_0 (counts)	I' (counts day^{-1})	A (counts)	P (days)	ϕ (rad)
A.....	32	3560 ± 710	0.05 ± 0.08	34.2 ± 6.0	41.8 ± 0.9	−1.6 ± 2.7
BCD.....	39	3200 ± 160	0.09 ± 0.02	−102 ± 12	82.5 ± 0.3	−0.4 ± 2.4
B.....	17	3070 ± 580	0.10 ± 0.06	−139 ± 9.5	82.7 ± 0.7	−2.8 ± 0.7
C.....	11	4250 ± 200	−0.02 ± 0.02	−34.5 ± 8.0	42.4 ± 0.2	−2.9 ± 1.3
D	11	5473 ± 645	−0.14 ± 0.06	−114.8 ± 16.3	84.3 ± 0.8	−1.5 ± 2.2

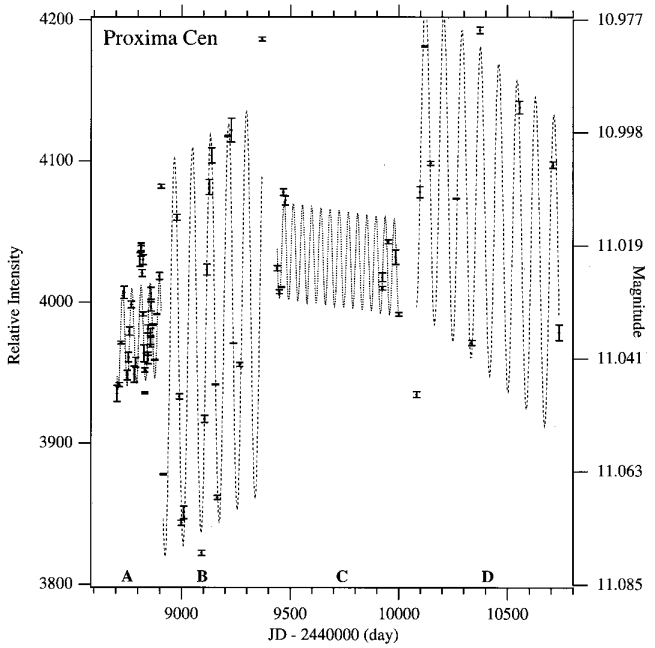

FIG. 13.—Direct light curve. Each symbol represents the average of from two to four exposures per orbit, with flares removed. Error bars are 1 σ. See Table 5 for the results of fitting a sine wave and trend (eq. [4]) to each segment.

the phase shift required to align the two long-period segments is small ($\Delta\phi = +0.11$) for the period $P = 83.5$ days suggested by the periodogram (Fig. 11). We have shifted segment D down by $\Delta S = -104.4$ counts. The bottom panel of Figure 14 shows a phased light curve for the two shorter period segments (A and C), phased also to $P = 83.5$ days. Shifts in phase and intensity to achieve alignment are indicated in the figure. The clean double sine wave also demonstrates that the low-amplitude segments, A and C, have half the period of the higher amplitude, longer period segments, B and D.

Finally, Figure 15 is used to demonstrate that the same low-amplitude, short-period variations seen in segments A and C may also be present in segments B and D. We fitted a sine wave to the phased B and D light curve in the lower panel of Figure 15, constraining the period to one cycle. The top panel of Figure 15 shows the residuals to that fit. These residuals are then fitted with a sine wave with the period constrained to one-half cycle. Comparing with the bottom panel of Figure 14, we find a similar double sine wave, nearly identical phase, and an amplitude ($A = 25 \pm 8$) close to that reported for segments A and C in Table 5.

4.2.2. *Barnard's Star Light Curve*

We turn now to the per-orbit average photometry of Barnard's star. Figure 16 (*bottom*) contains the per-orbit average direct light curve. The error bars are 1 σ, obtained from the dispersion of the three observations within each

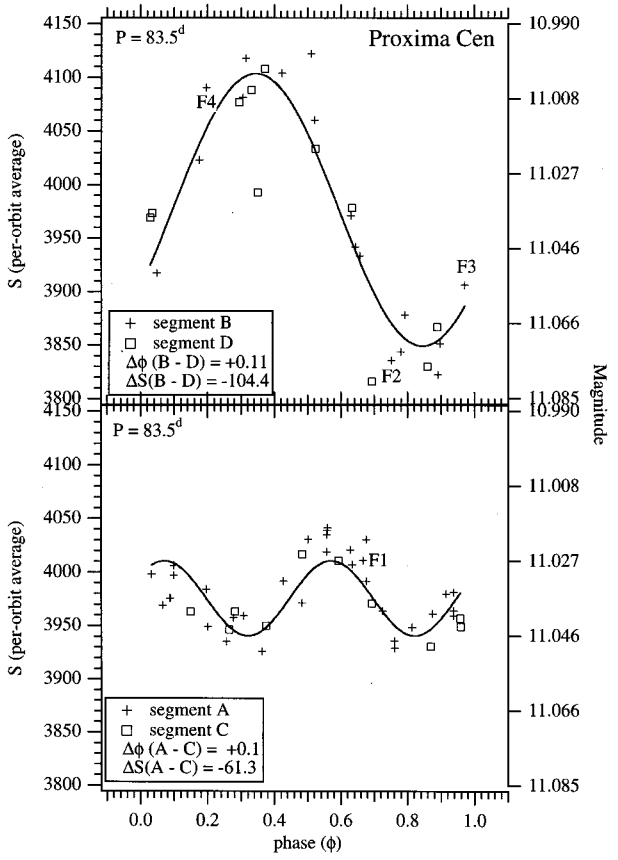

FIG. 14.—Phased light curves for Proxima Cen. *Top*: The two long-period segments (B and D; Fig. 13). The sine wave fit has a period constrained to one cycle. *Bottom*: The short-period segments (A and C) are phased to the longer period and show a double sine wave. The fit is constrained to have a period of one-half cycle. Error bars are about the size of the symbols. The observed flares are labeled F1–F4.

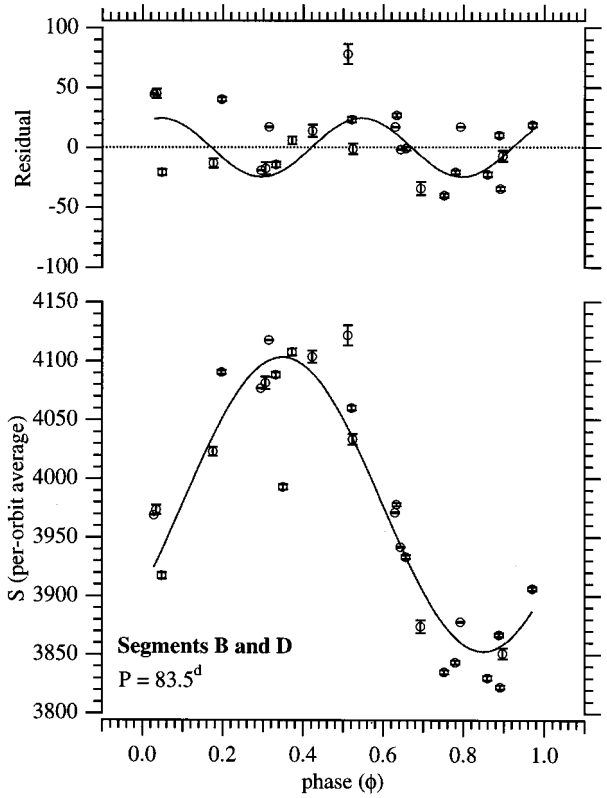

FIG. 15.—Phased light curve for Proxima Cen. *Bottom*: The two long-period segments (B and D; Fig. 13), phased to $P = 83.5$ days and fitted with a sine wave having a period of one cycle. *Top*: The residuals to the sine wave fit. These show a double sine wave pattern nearly identical to the two short-period segments, A and C (Figs. 13 and 14), suggesting that the low-amplitude, short-period signature persists during segments B and D.

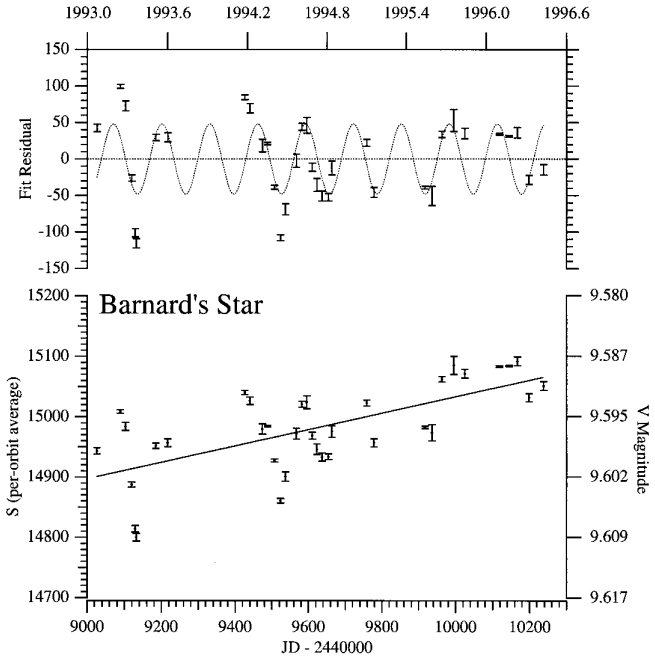

FIG. 16.—Per-orbit average direct light curve. Each symbol represents the average of three exposures. Error bars are 1 σ. *Bottom*, fitted with a trend line; *top*, residuals to the trend line, fitted with a constant-amplitude sine wave with constrained $P = 130.4$ days.

orbit on each date (Fig. 10). Residuals to a linear trend are presented in the top panel of Figure 16. The sine wave fit to these residuals was constrained to have the most significant period detected in the Figure 12 periodogram, $P = 130.4$ days. Figure 17 contains a light curve for the trend-corrected Barnard's star photometry of Figure 16 (*top*), phased to $P = 130.4$ days. The phased light curve is far less clean than for Proxima Cen. The periodogram and Figures 16 and 17 provide only weak evidence for periodic variation, primarily because of the poor sampling.

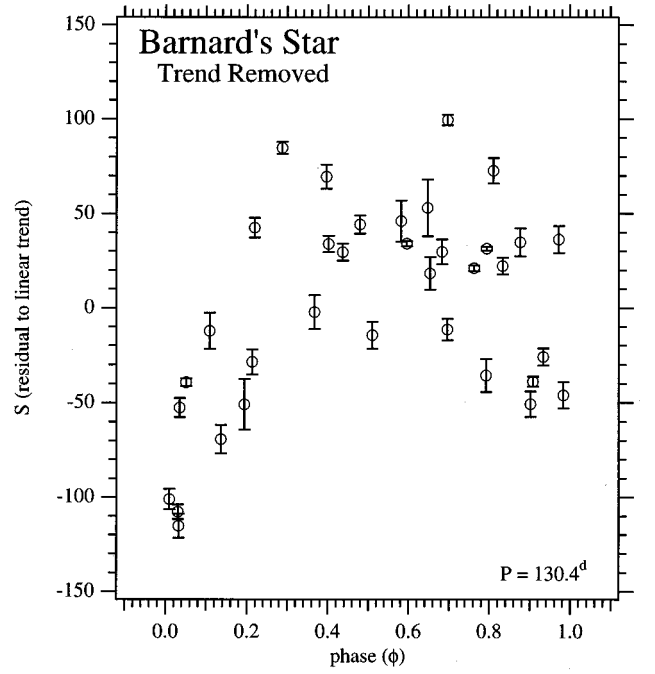

FIG. 17.—Trend-corrected light curve for Barnard's star, phased to $P = 130.4$ days. The full amplitude of the variation is ~ 0.01 mag. Error bars are 1 σ.

5. DISCUSSION OF PHOTOMETRIC RESULTS

Instruments can impress spurious periodicities on data (Kristian 1991). It is comforting that we find for all segments of either data set that $P_{\rm Barn} \neq P_{\rm Prox}$.

Stars have local imperfections in their atmospheres (e.g., the Sun; Zirin 1988). Stars other than the Sun have been shown to be spotted, photometrically (dwarf M stars; Kron 1952) and spectroscopically (e.g., Hatzes 1993; Neff, O'Neal, & Saar 1995). Other M stars have been shown to have spots, both dark (Bouvier et al. 1995) and bright (α Ori; Gilliland & Dupree 1996).

A spot on a rotating star is a model rich in degrees of freedom. Spots can be bright (plages) or dark (see Pettersen, Hawley, & Fisher 1992 for a discussion of the choice between dark spots on a bright background or bright spots on a dark background). Spots can wax and wane in size, driving the mean brightness level of a star up or down (Vrba, Herbst, & Booth 1988). Spots can migrate in latitude, which, when coupled with presumed differential rotation, can change the phasing and perceived rotation period. Spots are thought to migrate up or down (relative to the star's center) within the magnetosphere (Cameron & Campbell 1993), inducing perceived period changes. In the following sections we shall interpret the variations seen in Figures 13 and 16 as rotational modulation of spots or plages.

5.1. *Spots on Proxima Cen*

If we assume a fundamental rotation period $P = 83.5$ days, then variations in the amplitude (Fig. 13) could be due to spot/plage changes. With the sparse set of single-color photometric data presented in Figure 13, we have made no effort to quantitatively model spots (cf. Neff et al. 1996). The period and amplitude changes can be qualitatively modeled using plages and spots but require the disappearance of a feature or a major change in feature size or temperature in less than one rotation period (e.g., the A-to-B segment transition seen in Fig. 13).

Segments B and D (Fig. 14, *top*) require a single large or darker spot that reduces the average brightness of Proxima Cen by $\Delta V \sim 0.03$. This feature was not present in segment A and disappeared during segment C. To phase segments B and D, we applied a shift of $\Delta\phi = 0.1$ rad. Thus, the spot site lagged behind the fundamental rotation period by about 5° over the end of B–to–start of D time separation of ~ 700 days. Whether due to latitude migration coupled with differential rotation or from changes of height within the magnetosphere is unknown. If due to differential rotation, then either the spot moved very little in latitude or differential rotation on Proxima Cen is several orders of magnitude less than on the Sun (Zirin 1988).

Segments A and C exhibit smaller amplitude variations with a period almost exactly half that found for segments B and D. These segments (see the phased light curves in Fig. 14, *bottom*, and Fig. 15, *top*) could be produced by two smaller spots spaced 180° in longitude, carried around by the fundamental 83.5 day rotation period, and persisting through all segments, A to D. These two spots produce a $\Delta V \sim 0.01$. One of these small or less dark (warmer) spots lies at nearly the same longitude as the prominent spot seen in segments B and D. The other lies near the center of the brighter hemisphere in segments B and D.

From Figure 13, we note that the peaks in segments B and D were brighter. In segment B the minima were deeper, implying a darker (cooler) spot. To increase the amplitude of the maxima in segments B and D requires the existence of plages, or that the hemisphere not containing the single large spot became brighter as a result of spot changes. One of the pair of spots, associated with the brighter hemisphere ($\phi \sim 0.3$; Fig. 15, *top*), does have a shallower minimum than the other of the pair, at $\phi = 0.8$. If these are the same spots responsible for the variation in segments A and C, then the spot at $\phi \sim 0.3$ did have a shallower minimum in segments B and D (compare Fig. 14, *bottom*, and Fig. 15, *top*). However, that spot did not become less dark by enough to account for the increased maxima seen in segments B and D. As a consequence we propose plage activity to increase the segment B and D maxima.

Flaring activity seems more prevalent in segment B. As seen in Figure 14, three of four flares are grouped near phase $\phi = 0.8$. Association with this deep minimum might imply some connection of flaring activity with the largest or coolest starspot, which is also at the same longitude as one of the two smaller spots seen best in segments A and C. The remaining flare, F4, lies close to $\phi = 0.2$, the other spot of the low-amplitude pair of spots. Spot-flare association was previously noted in the M dwarf EV Lac, shown also to have longitude-dependent flaring associated with a starspot site (Leto et al. 1997). However, for EV Lac flares were detected a year before the spots became easily detectable by their system ($\Delta V \sim 0.1$), and, once spots formed, flare activity abated.

5.2. *A Small, Variable Spot on Barnard's Star*

The periodogram (Fig. 12) does not provide a clear identification of a single period of variation. The trend-corrected direct light curve (Fig. 16, *top*) has been fitted with a sine wave, constraining $P = 130.4$ days. The constant amplitude is $\Delta V \sim 0.01$, about 5 times our formal photometric error. Given the sparse coverage, it is speculative to interpret this light curve as showing rotational modulation of a single, small spot decreasing in size.

5.3. *Rotation Periods for Proxima Cen and Barnard's Star*

Rotation periods for Proxima Cen have been predicted from chromospheric activity levels by Doyle (1987), who obtained $P = 51 \pm 12$ days. Guinan & Morgan (1996) measured a rotation period ($P = 31.5 \pm 1.5$ days) from *IUE* observations of strong Mg II *h* and *k* emission at 280 nm. We find no support for either rotation period in our periodogram (Fig. 11) or light curves, direct (Fig. 13) or phased (Fig. 14). We do note that the variation due to the spot pair produces a period between the Doyle prediction and the Guinan & Morgan measurement.

The observed variations for Proxima Cen and Barnard's star, if interpreted as rotationally modulated spots, yield rotation periods far longer than for other M stars. For example, Bouvier et al. (1995) found 4 days $< P <$ 8 days for a sample of young, early M T Tauri stars. Magnetic braking is postulated to slow rotation over time (Cameron & Campbell 1993). The inferred rotation period for Proxima Cen is consistent with old age. This age may be 4–4.5 Gyr, if Proxima Cen is coeval with α Cen (Demarque, Guenther, & van Altena 1986). A relatively older age for Barnard's star can be surmised from lower than solar metallicity (Gizis 1997) and higher than solar space velocity (Eggen 1996), both consistent with a longer rotation period, if one accepts the reality of the variation.

5.4. *Shorter Timescale Variations*

The level of internal per-orbit precision for these photometric data is near 0.002 mag. Hence, the dispersion about the phased light curves for Proxima Cen (Fig. 14) is likely intrinsic to the stars. Two possibilities are miniflaring and the creation and destruction of small starspots and plages. That either phenomenon must have a duration longer than hours, at least for Proxima Cen, is suggested by the segment A phased light curve (Fig. 14, *bottom*) and a detailed light curve for segment A (see Benedict et al. 1993, their Fig. 3). Segment A contains four pairs of back-to-back orbits and one set of three contiguous orbits (on MJD 8,845). In each case the time-on-target coverage is over 90 minutes. For most of these contiguous orbits, differences are within 2 standard deviations and not statistically significant. Since "flare" implies a relatively short duration, miniflaring cannot be the cause of the scatter.

5.5. *Activity Cycles*

The $\sim$1100 day cycle of alternating high and low amplitude (see Fig. 13) is suggestive of an activity cycle for Proxima Cen. However, the gap in our coverage in segment C weakens any claims that can be made relative to the timing of this cycle. Comparing their 1995 *IUE* data with earlier archival data, Guinan & Morgan (1996) proposed an activity cycle that was in a low state in 1995, agreeing with our identification of segment C as representing a low state (Fig. 13).

6. CONCLUSIONS

1. For FGS 3 photometry, we have identified four sources of systematic error: background contamination (primarily zodiacal light), spatial flat-field variations (significant only for target positions $r > 20''$ from pickle center), temporal sensitivity changes (calibrated to a level introducing a 0.001 mag differential run-out error in 1000 days), and a possible warm-up effect (see § 3.3).

2. Two to four short ($t \leq 100$ s) observations with FGS 3 during one orbit yield 2 mmag precision photometry, provided the targets are bright ($V \leq 11.0$) and restricted to the central 20″ of the pickle.

3. Proxima Cen exhibits four distinct segments with two distinct behavior modes: short period, low amplitude and long period, large amplitude. These variations are consistent with a fundamental rotation period of $P = 83.5$ days and three darker spots. Two of the spots are either very small or very low contrast. They are spaced by 180° and persist throughout our temporal coverage, over 24 rotations. A single, more prominent spot (either large or high-contrast) formed in less than one rotation period, persisted through four rotations, and then disappeared. A spot reappeared within 5° of this same longitude five rotations later. The hemisphere opposite this spot brightened each time the spot formed. It is intriguing that active longitudes of spot formation separated by 180° are observed in chromospherically active stars with close stellar companions (Henry et al. 1995). If the photometric behavior of Proxima Cen is indicative of a synchronously rotating companion, its mass is less than that of Jupiter (Benedict et al. 1997).

4. We interpret the four distinct segments with two distinct behavior modes seen in the Proxima Cen photometry

as an activity cycle with a period of ~1100 days. Most of the flare activity occurred in the long-period, high amplitude variation segment B. In the phased light curve, three of the four detected flares are near the deepest minimum.

5. The scatter in the Proxima Cen phased light curve is far larger than our photometric precision. This scatter could be caused by the formation and dissolution of small spots or plages within one rotation period.

6. We find brightness variations 5 times our formal photometric precision for Barnard's star. Unfortunately, the sparse coverage of the possible variation renders it a marginal detection. We conclude that Barnard's star shows very weak evidence for periodicity on a timescale of approximately 130 days.

To confirm the spots and the inferred rotation periods will require observations of color changes (e.g., Vrba et al. 1988) and additional spectroscopic observations of lines sensitive to the presence or absence of starspots. Extended-duration millimagnitude V-band photometry from the ground, while difficult (Gilliland et al. 1993), could probe the activity cycle periodicity of Proxima Cen. Future tests could include *Space Interferometry Mission* (Shao et al. 1995) observations with several-microarcsecond astrometric precision. If spots and plages exist on these stars, we can expect easily detectable star position shifts as activity sites vary. Such observations will provide detailed maps of spot and plage location. Extended temporal monitoring will provide evolutionary details.

Support for this work was provided by NASA through grants GTO NAG 5-1603 and GO-06036.01-94A from the Space Telescope Science Institute, which is operated by the Association of Universities for Research in Astronomy, Inc., under NASA contract NAS 5-26555. We thank Bill Spiesman and Artie Hatzes for discussions and draft paper reviews and Melody Brayton for paper preparation assistance. Denise Taylor provided crucial scheduling assistance at the Space Telescope Science Institute. Suggestions by an anonymous referee produced substantial improvements to the original draft.

APPENDIX

This appendix contains the observation logs and measured average S-values for Proxima Cen (Table A1) and Barnard's star (Table A2).

TABLE A1

PROXIMA CENTAURI LOG OF OBSERVATIONS

MJD	Exposure Time (s)	Average Intensity (counts)
8,704.858.....	93.60	3972.96
8,704.871.....	66.45	3988.01
8,713.824.....	92.55	3971.07
8,713.838.....	66.45	4001.50
8,723.807.....	92.40	4015.08

NOTE.—Table A1 is presented in its entirety in the electronic edition of the Astronomical Journal. A portion is shown here for guidance regarding its form and content.

TABLE A2

BARNARD'S STAR LOG OF OBSERVATIONS

MJD	Exposure Time (s)	Average Intensity (counts)
9,025.634.....	80.4	15,065
9,025.649.....	24.3	15,046.7
9,025.658.....	24.3	15,064.8
9,088.103.....	50.25	15,106.1
9,088.117.....	24.3	15,116.5

NOTE.—Table A2 is presented in its entirety in the electronic edition of the Astronomical Journal. A portion is shown here for guidance regarding its form and content.

REFERENCES

Allen, C. W. 1973, Astrophysical Quantities (3d ed.; London: Athlone)
Benedict, G. F., et al. 1997, BAAS, 191, No. 70.07
———. 1994a, PASP, 106, 327
———. 1998, in ASP Conf. Ser. 154, The 10th Cambridge Workshop on Cool Stars, Stellar Systems, and the Sun, ed. J. A. Bookbinder & R. A. Donahue (San Francisco: ASP), 28
———. 1994b, BAAS, 185, No. 45.11
———. 1993, PASP, 105, 487
Bouvier, J., Covino, E., Kovo, O., Martín, E. L., Matthews, J. M., Terranegra, L., & Beck, S. C. 1995, A&A, 299, 89
Bradley, A., Abramowicz-Reed, L., Story, D., Benedict, G., & Jefferys, W. 1991, PASP, 103, 317
Cameron, A. C., & Campbell, C. G. 1993, A&AS, 274, 309
Cudworth, K. M. 1971, AJ, 76, 475
Demarque, P., Guenther, D. B., & van Altena, W. F. 1986, ApJ, 300, 773
Doyle, J. G. 1987, MNRAS, 224, 1P
Eggen, O. J. 1996, AJ, 111, 466
Gilliland, R. L., et al. 1993, AJ, 106, 2441
Gilliland, R. L., & Dupree, A. K. 1996, ApJ, 463, L29
Gizis, J. E. 1997, AJ, 113, 806
Gliese, W., & Jahreiss, H. 1991, Third Catalogue of Nearby Stars (Preliminary Version), in Selected Astronomical Catalogs, Vol. 1 (ADC/NSSDC CD-ROM) (Greenbelt, MD: GSFC)
Guinan, E. F., & Morgan, N. D. 1996, BAAS, 188, No. 71.05
Hatzes, A. P. 1993, ApJ, 410, 777
Henry, G. W., Eaton, J. A., Hamer, J., & Hall, D. S. 1995, ApJS, 97, 513
Henry, T. J., & McCarthy, D. W., Jr. 1993, AJ, 106, 773
Kirkpatrick, J. D., & McCarthy, D. W., Jr. 1994, AJ, 107, 333
Kristian, J. 1991, Nature, 349, 747
Kron, G. E. 1952, ApJ, 115, 301
Liebert, J., & Probst, R. G. 1987, ARA&A, 25, 473
Leto, G., Pagano, I., Buemi, C. S., & Rodonò, M. 1997, A&A, 327, 1114
Neff, J. E., O'Neal, D., & Saar, S. H. 1995, ApJ, 452, 879
Neff, J. E., Pagano, I., Rodonò, M., Brown, A., Dempsey, R. C., Fox, D. C., & Linsky, J. L. 1996, A&A, 310, 173
Panagi, P. M., & Mathioudakis, M. 1993, A&AS, 100, 343
Pettersen, B. R., Hawley, S. L., & Fisher, G. H. 1992, Sol. Phys., 142, 197
Press, W. H., Flannery, B. P., Teukolsky, S. A., & Vetterling, W. T. 1992, Numerical Recipes in FORTRAN (2d ed.; Cambridge: Cambridge Univ. Press)
Shao, M., Livermore, T. R., Wolff, D. M., Yu, J. W., & Colavita, M. M. 1995, BAAS, 187, No. 71.03
Vrba, F. J., Herbst, W., & Booth, J. F. 1988, AJ, 96, 1032
Walker, A. R. 1981, MNRAS, 195, 1029
Whipple, A., et al. 1995, in Calibrating *Hubble Space Telescope*: Post Servicing Mission, ed. A. P. Koratkar & C. Leitherer (Baltimore: STScI), 119
Zirin, H. 1988, Astrophysics of the Sun (Cambridge: Cambridge Univ. Press)